Q. J. R. Meteorol. Soc. (1990), **116**, pp. 317–335 551.509.5:551.515.13(265+267):514

Estimates of cyclone track predictability. II: Fractal analysis of mid-latitude cyclones

By KLAUS FRAEDRICH
Institut für Meteorologie, Freie Universität Berlin, West Germany
RICHARD GROTJAHN
Department of Land, Air, and Water Resources, University of California, U.S.A.
and
LANCE M. LESLIE
Bureau of Meteorology Research Centre, Melbourne, Australia

(Received 27 January 1989; revised 17 July 1989)

SUMMARY

A nonlinear systems analysis is applied to cyclone tracks over the North Pacific area (based on surface pressure analyses and twelve-hourly sampling time) and over the Australian region (based on 500 mb heights and daily sampling) for the respective winter seasons. First estimates are obtained of the degree of their chaotic or irregular behaviour in phase space and of the self-affinity of the planar tracks. This information is deduced from distance distributions (correlation integrals) between independent pairs of cyclone trajectories and from the structure function of individual cyclone paths.

The correlation integrals reveal average structures of the substitute phase space (such as the dimension of the attractor, a measure of predictability) after stratifying the North Pacific tracks into a western domain of growing and an eastern domain of large amplitude cyclones. A further subdivision into large-scale flow anomalies (the positive and negative Pacific/North America pattern in the eastern North Pacific) provides flow-dependent estimates which indicate two subsystems differing in dimension and predictability. The time scaling analysis of the planar cyclone paths characterizes systems of no scale preference: the associated variance spectra decrease by a 2 to 3 power law with increasing frequency.

1. INTRODUCTION

During the past twenty-five years or so, numerical weather prediction models have shown a steady increase in skill, especially in the first few days. Moreover, medium range forecasts are now exhibiting skill out to six or seven days. However, it has been recognized for some time that there are limits to the predictability of the atmosphere (Thompson 1957; Lorenz 1969; Smagorinsky 1969). Estimates for error doubling times of initially small errors are 2 to 5 days and estimates of the predictability limit of the atmosphere range between 8 and 14 days (Smagorinsky 1969). Beyond the limit of predictability, synoptic-scale features are no longer predictable by purely deterministic methods.

Despite the growing number of predictability studies in recent years (see for example Shukla 1984; Kalnay and Livezey 1985) the question of the predictability of particular types of meteorological systems has not been a major area of research. Most work on atmospheric predictability has concentrated on attempts to achieve the following aims: to reach as close as possible to the limit of predictability; to extend the limit on deterministic models by forecasting temporal and spatial mean values of the fields; and to provide *a priori* predictions of the forecast skill of deterministic models (Kalnay and Dalcher 1987).

Short term and medium range forecasts (1 to 10 days ahead) have to deal with a number of types of weather systems, such as tropical and extra-tropical cyclones, cold fronts, cut-off lows, jet streaks, etc., each of which may have a distinct growth rate for initially small errors. It is of paramount importance, therefore, to determine the error growth rates and predictability time scales for such systems. On a given day only a few systems are present and these are the major feature of interest in the forecast.

In the past decade, new techniques have become available for the study of atmospheric predictability. These techniques may be grouped under the general term 'nonlinear or dynamical systems analyses'. For a review see, for example, Eckmann and Ruelle (1985). An application to the predictability of the weather and climate system is given by Fraedrich (1987).

In part I of this investigation (Fraedrich and Leslie 1989) techniques of nonlinear systems analysis were applied to tropical cyclone tracks in the Australian region. Estimates of dimensionality and error growth rates (entropy) were obtained using about 250 tropical cyclones and it was found that the dimensionality is between 6 and 8 and that the e-folding error growth time scale is about 24 hours. These findings suggested that one to two days is the deterministic limit of predictability for tropical cyclones in the Australian region.

The present study concentrates on mid-latitude cyclone tracks in two very different parts of the world, the North Pacific area and the Australian Southern Ocean region. The phase space scaling techniques used in part I are applied to long term data sets to obtain estimates of dimensionality and growth rates of initially small errors. In addition, time scaling methods are applied (Mandelbrot 1982; see also Monin and Yaglom 1975; Lovejoy and Schertzer 1986) to the planar cyclone paths to analyse the self-affine structures of the tracks, their dimension and the power-law behaviour of their spectra.

In sections 2 and 3 the data sets and the methods of analysis used in this study are described. In section 4 the results are discussed for the North Pacific and Australian region cyclone tracks. Special emphasis is given to the differences between the western and eastern North Pacific basins and to a stratification of the cyclone tracks in terms of the governing large-scale flow anomalies such as the Pacific/North American and Western Pacific patterns.

2. Data

The positions of the mid-latitude cyclones in this study were obtained from data sets covering two different parts of the globe: the North Pacific region and the Australian Southern Ocean region.

(*a*) *North Pacific cyclone track data*

The North Pacific winter (January and February) cyclone tracks were calculated by a fully-automated procedure at the National Center for Atmospheric Research (NCAR) from sea-level pressure fields at 12-hour intervals. They were available at NCAR from the U.S. Navy archives. The original data are archived on a polar stereographic grid covering most of the northern hemisphere. Some details of the time and space interpolation scheme applied are described in the appendix; the estimated resolution is about 50 km.

In this study we concentrate on cyclone tracks that originate and reside within the North Pacific region. Most of these cyclones remain within an area which extends from 120°E to 235°E and from 20°N to 70°N (except for a line from 120°E 50°N to 150°E 70°N) and which, in the following, will be labelled the North Pacific basin. Very few cyclones enter this region from outside and only a fraction exits the eastern boundary of the domain. The primary reason for the choice of these boundaries is to delete mature storms over northern Siberia that come from Europe, and to delete storms which form over the Rocky Mountains (but reach maturity well outside). In short, we attempt to follow the complete life-cycles of maritime mid-latitude cyclones. When interpolated to 2-hour intervals, the number of storm centres for the 29 winter months studied amounts to

38 717 points within the North Pacific domain, which correspond roughly to 300 individual storms lasting longer than 3–4 days. A small sample is presented from the winter months January 1977 and 1982 (Fig. 1).

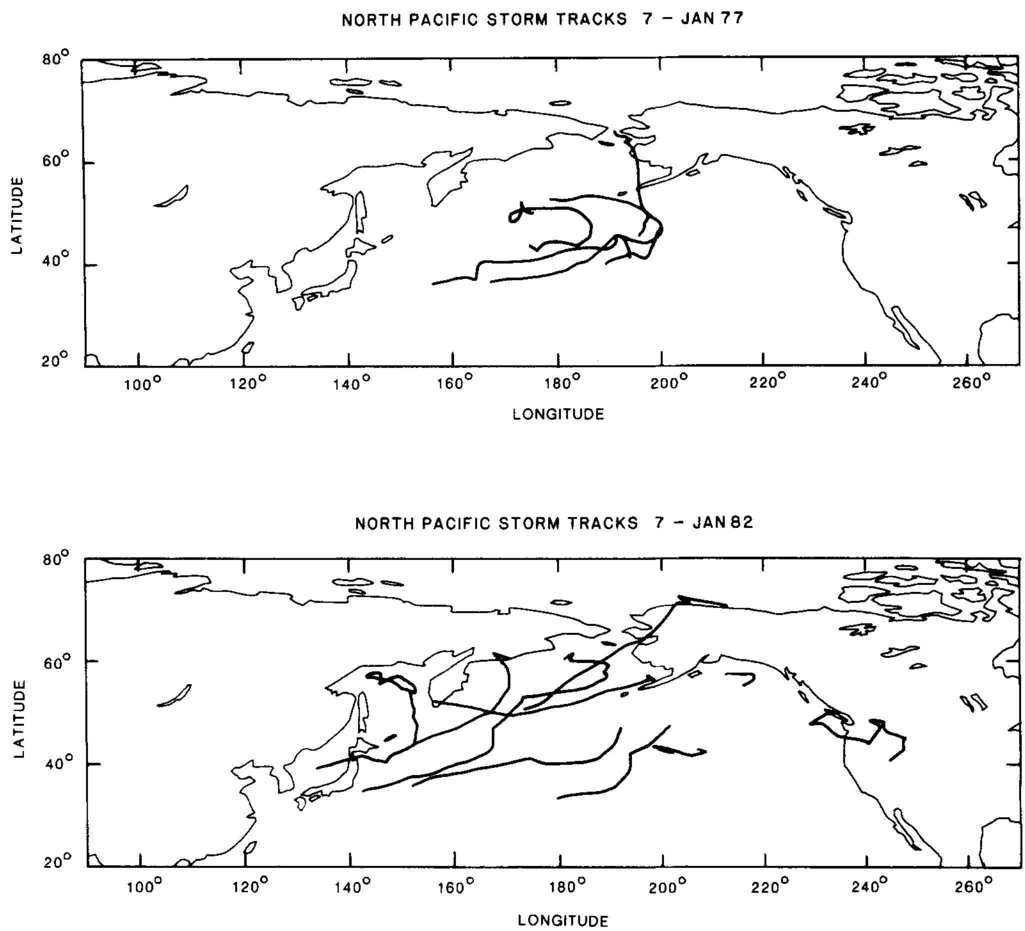

Figure 1. Representative North Pacific cyclone track samples from the winter months January 1977 (top) and 1982 (bottom).

(*b*) *The Australian region mid-latitude cyclone track data*

The cyclone track data were selected from a subdomain of the Australian region (Fig. 2) archived daily 500 mb analyses. A total of 150 cyclone tracks was selected, for the ten winter periods (June, July, August) from 1978 through 1987. The particular subdomain chosen covered roughly the area between latitudes 35°S and 50°S and longitudes 100°E and 160°E. The cyclone track centres were defined by the minimum values of the 500 mb height field. Only those cyclones with closed inner contours were selected. Troughs were not included. A small sample of Australian region mid-latitude cyclone tracks is presented in Fig. 2 for the winter months July 1982 and 1983.

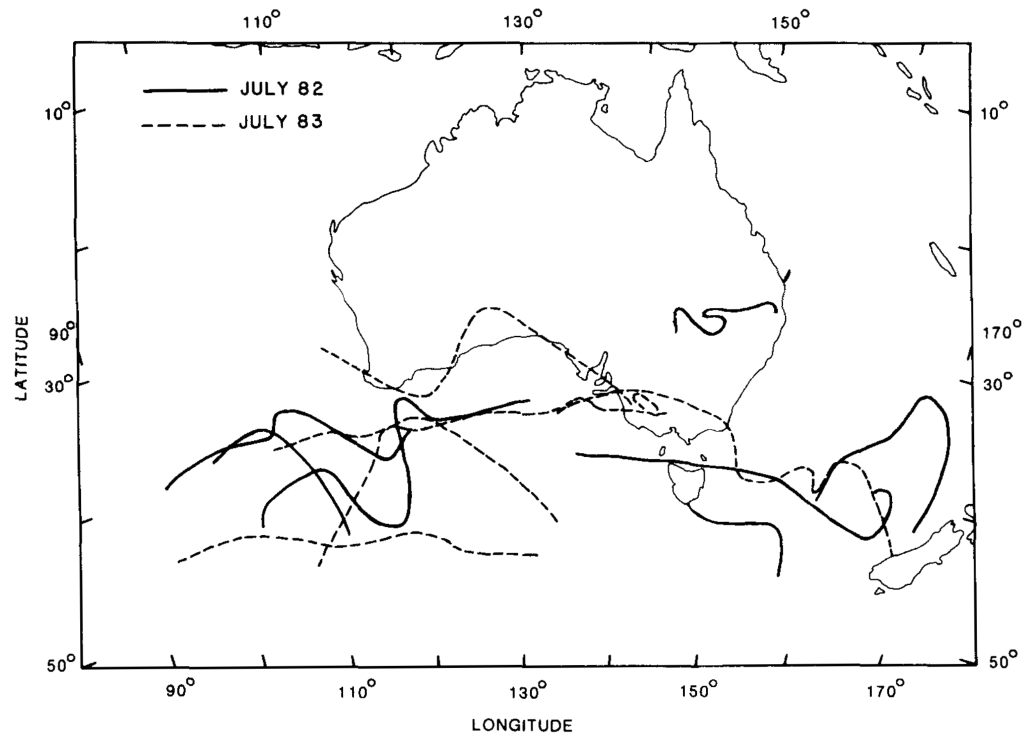

Figure 2. Australian region cyclone track samples for the winter months July 1982 and 1983.

3. Motivation and Methodology

The predictability of a dynamical system is a measure of the rate at which initially small errors grow. This measure can be obtained from phase space trajectories representing the time evolution of the system. A suitably averaged divergence of initially close trajectory pieces gives such a measure of predictability, because two initially close states (one being the true and the other the erroneous one) follow different trajectories through the phase space.

For the phase space of the system which governs the cyclone dynamics a substitute phase space is considered; it is spanned by delay coordinates which are defined by time-lagged planar cyclone track pieces. This substitute phase space is constructed to embed the cyclone attractor on which the cyclone dynamics evolves. Its dimension is $2m$, where the embedding m is the number of time lags involved representing the duration of the sections of a cyclone track. Thus, a point in this substitute phase space of delay coordinates is equivalent to a piece of a cyclone trajectory, and a trajectory in this phase space is a sequence of successive pieces of one and the same cyclone track. For a sufficiently large m relevant measures of static and dynamic properties of the embedded cyclone attractor can be estimated applying nonlinear systems analysis techniques in the substitute phase space. This leads to the dimension and the entropy of the cyclone attractor. That is, the number of active modes involved and the predictability. The first describes the fractal structure or strangeness of the attractor of the dynamical system, the latter is a measure of the degree of chaotic behaviour because it characterizes the system's sensitive dependence on initial conditions.

Two kind of nonlinear systems analysis technique will be employed in this investigation: one based on phase space scaling and the other on time scaling. The basic concepts and the phase space scaling part of the methodology applied here has been described by Fraedrich and Leslie (1989) and will be outlined only briefly. The analysis is based on the scaling of the trajectories in the substitute phase space of the dynamical system, which is spanned by 'delay' or 'lagged' coordinates. In addition to this phase space scaling, by which the correlation dimension and the order-2 entropy can be determined, a time scaling (applicable to self-affine systems) will also be made.

(a) *Phase space scaling*

Estimates of the order-2 entropy K_2 and the correlation dimension D_2 are obtained from the Grassberger–Procaccia (1984) algorithm, which is applied to the cyclone track position vector $X(t) = (x(t), y(t))$. They are analysed in a substitute or embedding phase space spanned by delay coordinates of

$$X_m(t_i) = [X(t_i), \ldots, X(t_i + (m-1)T)] \tag{3.1}$$

where the delay is an integral multiple of the sampling time T. For example, $m = 1$ refers to all individual points, $m = 2$ refers to all trajectory pieces which consist of two successive points, $m = 3$ represents all trajectory pieces of three successive points, etc., on independent cyclone tracks. In this sense $2m$-dimensional cyclone phase spaces are spanned by the delay-coordinates (3.1), in which a point represents a piece of a cyclone track (commencing at t_i), two successive points define a piece of the same cyclone track and the same length m, but shifted by one time step T; that is, they commence at t_i and $t_i + T$, etc. Thus cyclone dynamics evolves in a $2m$-dimensional phase space of time-shifted coordinates which define a substitute for the more common meteorological phase space of multi-variable coordinates. This substitute phase space embeds the observed dynamics (see for example Fraedrich 1987). Note, however, that owing to the finite life time of the cyclones, the substitute phase space may provide only an incomplete embedding of (the attractor of) the dynamical system. Summarizing this first step: Richardson's famous experiment of initially close parsnips diverging on the 2-dimensional sea surface (referee's personal communication) is now happening with close pieces of trajectories in the $2m$-dimensional substitute phase space spanned by pieces of cyclone tracks of duration mT. For sufficiently large embedding this substitute phase space embeds the (attractor of the) cyclone track dynamics.

Applying nonlinear systems analysis, the correlation integral, $C_m(l)$, has to be evaluated. This is the distribution function for the number, $N_m(l)$, of initially close pairs of pieces of independent or different cyclone trajectories $X_m(t_i)$, $X_m(t_j)$, whose great circle distances, $d_{ij}(k)$, remain less than a threshold l apart from one another while the tracks proceed with time, $0 < kT < (m-1)T$, from (t_i, t_j) to $(t_i + (m-1)T, t_j + (m-1)T)$. Plotting $C_m(l) = N_m(l)/(N_m - 1)^2$ in a $\ln C_m(l)$ versus $\ln l$ diagram, the required estimates of the correlation dimension, D_2, and the entropy, K_2 can be deduced from the scaling

$$C(l) = l^D \qquad \text{and} \qquad K_2 = (1/T)\exp(C_m/C_{m-1}) \tag{3.2}$$

for $l \to 0$ and $m \to \infty$; N_m is the number of cyclone tracks involved in the counting algorithm. The order-2 entropy, K_2, is a measure of the rate of divergence of initially close pieces of independent trajectories (that is, for the limit $l \to 0$), and thus a measure of predictability. The dimensionality, D_2, is a measure of the degrees of freedom which govern the underlying dynamics. The entropy and dimensionality estimates represent averages over that part of the weather attractor in phase space, which the cyclone tracks are able to cover during their life-cycle. The estimates from empirical data need to be made in a meaningful l range (Eckmann and Ruelle 1985). For l too small there are insufficient statistics, whereas for l too large the information is affected by nonlinearity. An intermediate range $l_1 < l < l_2$ of constant slopes $\ln C_m(l)/\ln l$ provides a statistically useful distribution of distances between the pairs of points in phase space.

Summarizing this second step: In the $2m$-dimensional substitute phase space we deduce the average number of points in any ball of given size. That is, we count the number of all points within a given distance, $d_{ij} < l$, from a base point in the substitute phase space; these points represent pieces of cyclone tracks in the neighbourhood of but independent of the base point. This counting algorithm is applied such that all points become base points to obtain an optimal sample size from the data available. The numbers counted in a ball of given size are averaged over all pieces of cyclone tracks or base points and normalized by the total number of points. This leads to an estimate of the probability of finding one pair of points in a ball of given radius and dimension: the correlation integral $C_m(l)$. Given an embedding m, a double logarithmic plot of the cumulative probability estimates, $\ln C_m(l)$, versus the increasing size of the ball (or distance threshold l), $\ln l$, (see Fig. 3) provides the basis of the analysis:

(i) At fixed embedding m the probability (of finding two independent cyclone track pieces close to one another) increases with the size of the balls. After a sufficiently large embedding this rate of change has reached a saturation value. Thus, (a) the substitute phase space can be assumed to embed the cyclone track attractor sufficiently so that, (b) the rate of change provides a measure of the order-2 dimension of the system and the number of active modes involved in its dynamics.

(ii) At fixed radius of the ball (or distance threshold) and with increasing embedding (by which the lengths of all trajectory pieces are simultaneously extended) the change of probability is a measure for pairs of trajectories (that is pairs of points in the substitute phase space) escaping from a ball of size l. This is the average divergence of a pair of pieces of cyclone trajectories in the substitute phase space; that is the predictability (or order-2 entropy; for more details see Fraedrich 1987; Fraedrich and Leslie 1989).

Alternatively, one may envisage the divergence as the average rate by which a trajectory leaves its (independent) base companion, after both have been identified to move on the attractor (after the embedding has reached saturation). Note that in analysing storm tracks we are introducing a $2m$-dimensional embedding based on a delayed vector variable in comparison with the more common analysis of scalar variables. This enhances the reliability of dimension and entropy estimates requiring 10^D independent data points which is satisfied for attractors of relatively low dimensionality. Note also that the probability of finding points in the smallest balls is relatively low and may not change with their size; in that case small horizontal bars appear at the bottom of the $C_m(l)$ graphs (Fig. 3).

(*b*) *Time scaling*

The structure function (or the variance of increments) can be estimated from each of the position components x or y of the cyclone tracks in the two-dimensional plane. In the case of self-affinity (see for example Mandelbrot 1982; Voss 1988), the structure function scales like

$$\langle (x(t + \lambda T) - x(t))^2 \rangle = \lambda^{2H} \langle (x(t + T) - x(t))^2 \rangle \tag{3.3}$$

where the delay time, λT, is an integral multiple of the sampling time, T; the average $\langle\ \rangle$ is taken over all cyclones individually and their life-cycle t. This relates the (squared) zonal or meridional distances travelled by a cyclone with its travel-time λT. The power-law relation between time and distance can be deduced from a double-logarithmic graph (Fig. 4). The x and y components may lead to different scaling exponents H_x and H_y. It characterizes a self-affine signal; that is, when the time scale is multiplied by a factor, λ, then the signal amplitude is multiplied by λ^{-H}, and the transformed time series has the same statistical properties as the original one.

The scaling can be related to the spectral time series analysis. As self-affinity implies that there is no preferred scale in the signal, the power spectrum follows a power law of the frequency f

$$P(f) = f^{-a} \quad \text{with} \quad a = 2H + 1 \tag{3.4}$$

(see for example Monin and Yaglom 1975). Note that in the case of cyclone tracks, the associated spectrum is based on a Lagrangian (and not the common Eulerian) frame. For the special case of self-similar fractals ($H_x = H_y$), the fractal dimension D of the trajectory in the plane is given by

$$D = \min(1/H; 2). \tag{3.5}$$

For small deviations from self-similarity one assumes $\langle H \rangle = (H_x + H_y)/2$.

4. Results and discussion

The methods described in section 3 are applied to the mid-latitude cyclone tracks in (a) the eastern and (b) the western North Pacific and (c) the Australian region, to obtain measures of the structure of the cyclone track attractor, (i) in an average sense, and (ii) for anomalous flow patterns; more specifically, of that part of the cyclone track attractor which is covered by the cyclone trajectories during their life cycle.

4.1. Phase space scaling

(a) *The eastern North Pacific*

(i) *Averaged estimates.* A first analysis of the 1758 cyclone tracks is designed to obtain average dimensionality and entropy estimates in the eastern (907 cyclones) and western (851 cyclones) parts of the North Pacific domain and the basin as a whole. The dividing line between the two parts was set at 180°E. This division was made for two reasons. First, because most storms form near the western edge of the basin. By the time they reach the eastern part most storms have attained large amplitude. Lau (1978) used smaller longitudinal sectors (of 40° to 50°) for this reason with a dividing line at 150°E. The second reason is to separate the North Pacific into two regions, each mainly influenced by only one climate anomaly pattern.

A quick glance at the storm tracks during most months reveals that the tracks of developing cyclones (western North Pacific) tend to move in parallel toward the east-north-east (see also Fig. 1). During these formative stages, the lows tend to be advected along by the long wave and zonal flows. Further downstream (eastern North Pacific) the flow is more perturbed and the nonlinear motion is more erratic. Since the analysis is concerned with close pairs of trajectory pieces, we might expect lows in the western part of the basin to be distinctly less complex (and more predictable) than those in the eastern domain. On the other hand, lows move more rapidly in the western region; even though the motion may be more parallel, proportional variations about the faster flow could lead to lesser predictability. In the following discussion we will concentrate mostly on

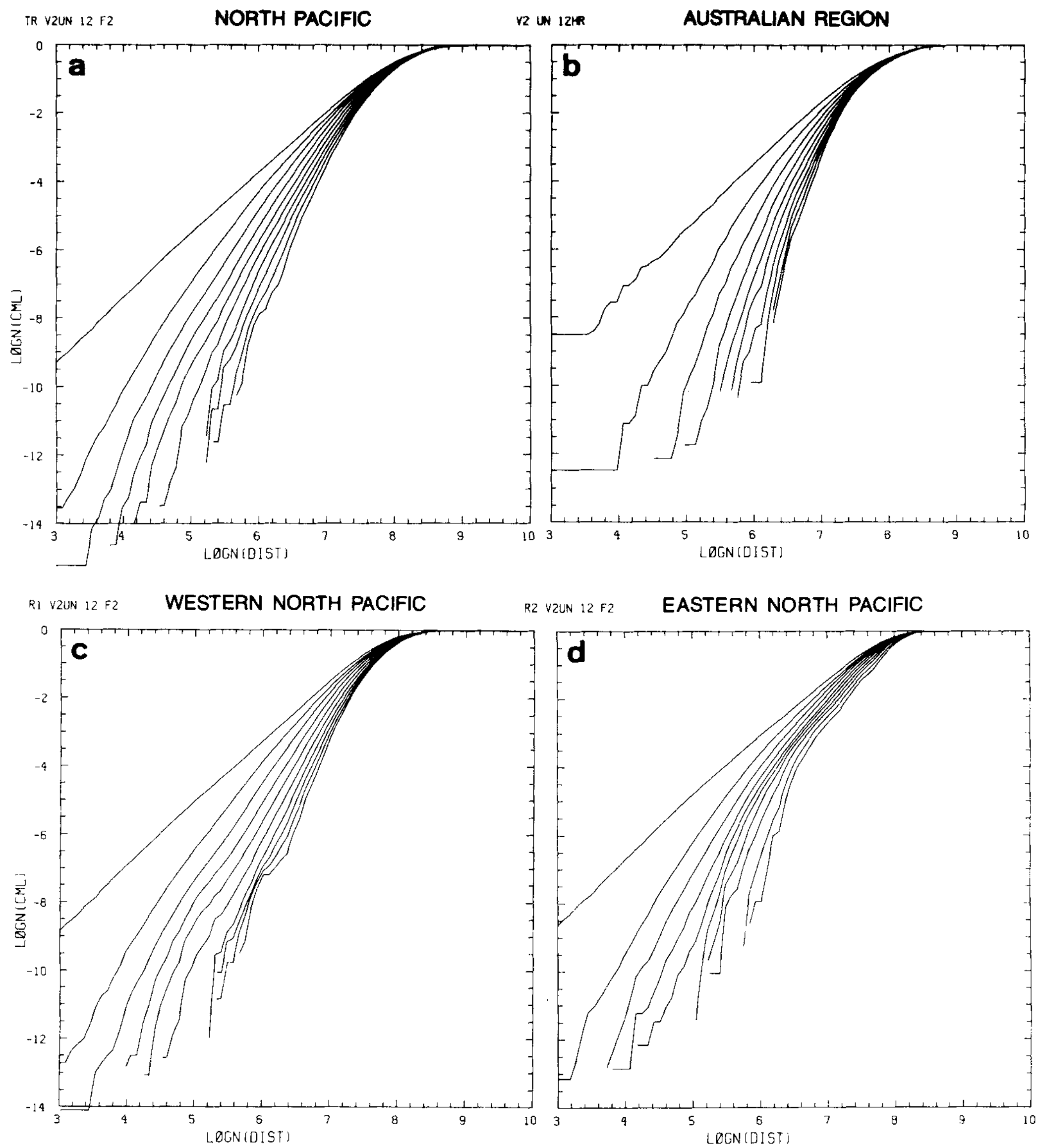

Figure 3. Correlation integral or cumulative distance distributions $C_m(l)$ of pairs of independent cyclone trajectory pieces displayed in ln $C_m(l)$ versus ln l diagrams (the label logn denotes the natural logarithm). Each curve is for m times the number of data time steps ($m = 1$ to 10, from left to right in each diagram). Except for (b) the time step used is twelve hours. Cyclone tracks are analysed for the total, western and eastern North Pacific basin (a, c, d); daily time steps are used for the Australian region (b). Positive and negative index PNA patterns of the eastern North Pacific (e, f) are also presented.

the eastern North Pacific basin, where the more interesting results were obtained, in particular when comparing average with anomalous circulation patterns.

The correlation integrals, $C_m(l)$, of the eastern (and western) storm tracks are calculated for cyclones which last longer than 36 hours; they are based on a sampling time of $\tau = 12$ hours and a delay or lag up to $m = 10$. The $C_m(l)$ graphs are displayed in a ln $C_m(l)$ versus ln l diagram to estimate the entropy and dimensionality, Eq. (3.2), of the underlying dynamics in a meaningful distance range. The eastern domain reveals the

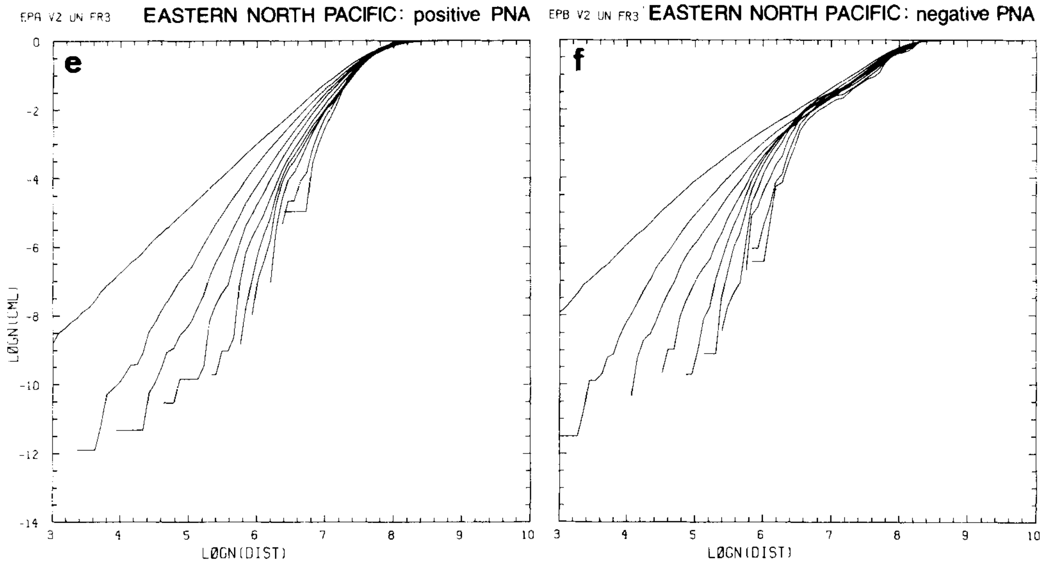

Figure 3 (continued).

most interesting structure (Figs. 3(d) to (f)) which also differs from analyses of storm tracks in the tropics or in the antarctic region (Fraedrich and Leslie 1989). The following results (compiled from Fig. 3) are noteworthy:

Firstly, in the distance range 700 km $< l <$ 2500 km (ln(dist) = 6·5 and ln(dist) = 8 in Fig. 3), we observe that a saturation value is reached for the slopes of the $C_m(l)$ graphs when increasing the embedding dimension of the substitute phase space. That is, the dimensionality of the dynamical system, which governs the tracks of cyclones for this relatively large range of scales, does not increase beyond $D_2 = 2$ to 2·5 when the embedding or delay time rises from $m = 5$ to $m = 10$ ($2m$ is the substitute phase space dimension). This slope is observed over 2–3 orders of magnitude. The related entropy estimates $K_2 = (\ln C_5 - \ln C_8)/36$ hours $= 1/120$ hours correspond to an error doubling time of 3–4 days, which appears to decrease with higher embedding m.

Secondly, at distances $l = 700$ km (ln(dist) = 6·5 in Fig. 3), however, there is an indication of a 'knee' or change of curvature in the $C_m(l)$ graphs for larger embedding dimensions ($m > 6$) associated with a change of the scaling exponent D_2. That is, for the smaller distance scales $l < 700$ km the $C_m(l)$ slopes continue to increase with increasing embedding dimension. The dimensionality associated with these smaller scales does not appear to reach a saturation value and the entropy (unpredictability) rises. This indicates a high degree of randomness and/or a high dimensional attractor subset for that part of the dynamics which cannot be captured by this analysis. Whereas for larger distance scales ($l > 700$ km) the scaling exponent D_2 tends towards saturation. A possible explanation is that the regime of the smaller scales may be characterized by geostrophic turbulence.

The following interpretation is suggested to explain the existence of such a knee (see Eckmann and Ruelle 1985): The attractor of the observed cyclone process may consist of two subsystems. The subsystem with the lower dimensionality and longer predictability is related to the larger distance scales $l > 700$ km, which is associated with Rossby dynamics. In the smaller-scale domain the complete system contributes to the estimate of dimensionality and predictability. Two conclusions are possible: The larger-scale (and low-dimensional) subsystem drives (slaves) the smaller scale (of, say, geostrophic turbulence). Or noise effects are so large that they dominate all but a fraction of the attractor. That is, the deterministic dynamics is covered under the noise in the data, and only the largest amplitudes are recognized as deterministic signals. How or whether this can be related to the existence or non-existence of a slow manifold (Lorenz 1986; Lorenz and Krishnamurty 1987) cannot be deduced by this dynamical systems analysis method; that is, a correspondence of the larger-scale subsystem with the slow manifold Rossby modes and of the smaller scales with the inertial gravity modes is only speculative. Note that it cannot be ruled out that the observation of a smaller-scale subsystem is a manifestation of the larger scale ($l > 700$ km) Rossby mode dynamics affected by noise and/or geostrophic turbulence ($l < 700$ km). Noise is inherent in the observations due to the finite data resolution in space and the storm track interpolation scheme; about twice the grid distance at 60° latitude is close to 700 km. Thus observational or interpolation errors, noise and/or geostrophic turbulence are realized up to a scale of $l = 700$ km.

Finally, this scale separation in the eastern North Pacific cyclone track dynamics is observed as an average over all large-scale circulation patterns under which cyclones occur. Therefore we need to investigate next whether this structure can be related to one particular large-scale circulation anomaly, which may persist in the eastern North Pacific area, or whether it is a general feature of the mature large amplitude cyclones in the eastern Pacific.

(ii) *Anomalous flow patterns.* The characteristics of anomalous, persistent flows have been indentified and classified by climate research in recent years. A prime example of an anomalous circulation affecting the eastern North Pacific is the 'Pacific/North America' (PNA) pattern identified by Wallace and Gutzler (1981), elements of which have been noticed for many years (Allen *et al.* 1940; Namias 1951); Dickson and Namias (1976) were apparently the first to show the whole PNA pattern. In the western North Pacific a north–south see-saw has been identified which Wallace and Gutzler refer to as the western Pacific (WP) pattern, which fits well into our domain. Such different structures of the mean flow reflect fundamental differences in the motion, dimension, predictability and other dynamical properties of the individual cyclones. If such a connection can be established, then the usefulness of these classifications would be greatly enhanced.

The PNA index is positive (PNA > 0) when the Aleutian low is deeper and the ridge over Canada is stronger, which seems to enhance the climatological long wave structure in the region (and *vice versa*, PNA < 0). The deeper Aleutian low may arise from more intense storms in the region or less motion of the lows. The PNA pattern is primarily in the eastern North Pacific region but is recognized to extend well east of our North Pacific basin. The 'Canadian high' of the PNA is centred close to the eastern edge of our domain. Months of prominent PNA pattern are selected on the basis of their indices (Nakamura, personal communication) and given in Table 1. These indices overlap with and extend the time frame of those published by Wallace and Gutzler. Usually the published indices agree in sign and magnitude with those provided by Nakamura. The sign convention is the same, but the method of calculation is somewhat different (Nakamura *et al.* 1987). Lau (1988; L) and Grotjahn and Lai (1989; GL) have examined how the storm tracks vary for different values of the WP and PNA indices. For the eastern Pacific, L and GL find contrary deflections of the storm tracks caused by the PNA anomaly. For negative PNA GL find the storm track at 180°E further south, but L further north, which may be ascribed to differing approaches: GL include cut-off lows that persist in the Gulf of Alaska, whereas L largely excludes them. For negative PNA there seem to be fewer quasi-stationary cut-off lows in the Gulf than for positive PNA. Since negative PNA is associated

TABLE 1. MONTHLY TELECONNECTION PATTERN INDICES

Year	Pacific/N.A. index		West Pacific index	
	January	February	January	February
1972	−1·46	−0·68	−0·90	1·21
1973	−0·04	0·52	−1·48	−0·91
1974	−0·74	−0·28	2·50	−0·33
1975	−0·83	−0·39	−0·85	−0·32
1976	0·44	−1·14	0·21	−0·58
1977‡	1·97	1·78	1·17	−0·53
1978	1·47	2·10	0·07	0·18
1979	0·39	−1·25	−0·99	−0·42
1980	0·18	1·83	1·59	0·44
1981	2·71	0·33	0·84	0·74
1982‡	−0·56	−0·88	0·03	1·63
1983	1·78	2·12*	0·20	0·39*
1984	0·63	0·62	1·50	0·19

* Sea level pressure data not available
‡ January cyclone tracks displayed in Fig. 1

with greater barotropic instability (Palmer 1988), we might expect storms to grow more readily in the eastern Pacific. When PNA is negative, GL find that the width of the storm track is significantly larger than for positive PNA (or either sign of WP). The greater spread of these storm locations can be seen even for the brief period shown in Fig. 1 (PNA >0 in January 1982). The greater spread is one reason why our negative PNA results differ from the other examples. The width of the storm track is not always broad for negative PNA, noi is it always narrow for positive PNA; however, this relation holds frequently enough to be statistically highly significant. Accordingly we select two groups (Table 2, labelled EPA and EPB) with the PNA index $>0{\cdot}4$ and $<-0{\cdot}4$ to analyse storm tracks in the eastern North Pacific basin.

The phase space scaling leads to the following results for the correlation integrals which are associated with the negative (342 cyclones) and positive (207 cyclones) index PNA patterns:

The negative index PNA pattern (EPB: PNA $<-0{\cdot}4$) exhibits two subsystems controlling the storm track dynamics. Both the negative index and average circulation analyses reveal the scale separation near the same distance scale, $l = 700$ km.

The larger-scale subsystem (700 km $< l <$ 2900 km) of the negative index months shows a dimensionality $D_2 = 1{\cdot}2$ to $1{\cdot}4$ which, despite considerable fluctuations, lies below

TABLE 2. MONTH/YEAR OF POSITIVE ($>0{\cdot}4$) AND NEGATIVE ($<-0{\cdot}4$) CIRCULATION INDICES OF THE PACIFIC/NORTH AMERICA (PNA) AND WESTERN PACIFIC (WP) PATTERNS

Eastern North Pacific region and PNA pattern:		
EPA:	PNA $> +0{\cdot}4$ (11 months): (342 cyclones)	2/73, 1/76, 1/77, 2/77, 1/78, 2/78, 2/80, 1/81, 1/83, 1/84, 2/84
EPB:	PNA $<-0{\cdot}4$ (8 months): (207 cyclones)	1/72, 2/72, 1/74, 1/75, 2/76, 2/79, 1/82, 2/82
Western North Pacific region and WP pattern:		
WPA:	WP $> +0{\cdot}4$ (9 months): (268 cyclones)	2/72, 1/74, 1/77, 1/80, 2/80, 1/81, 2/81, 2/82, 1/84
WPB:	WP $< -0{\cdot}4$ (8 months): (244 cyclones)	1/72, 1/73, 2/73, 1/75, 2/76, 2/77, 1/79, 2/79

that obtained from the average eastern North Pacific analysis. The related predictability estimate based on the order-2 entropy can only be considered as a very weak bound, $1/K_2 < 5$ days, corresponding to an error doubling time of about 3 days. It is deduced in the neighbourhood of $C_m(l = 700\text{ km})$ and comparable with the averaged estimates; there is an indication for decreasing predictability time scale with higher embedding m.

The smaller-scale subsystem ($l < 700$ km) shows increasing dimensionality ($D_2 > 7$) and reduced predictability ($1/K_2$ about 1 day) for growing embedding dimension or delay time (m). Note, however, the relatively low number of months on which the statistics are based.

The positive index (EPA: PNA > 0·4) results indicate a greater dimensionality of the larger-scale subsystem (700 km $< l <$ 2000 km), $D_2 = 2{\cdot}7$ to $2{\cdot}9$, than the negative index and average analyses; the predictability, $1/K_2 = 3$ days, is calculated in the neighbourhood of $C_m(l = 700\text{ km})$. Note that this larger-scale subsystem appears vaguely in embeddings $5 < m < 8$ and only over a relatively small scaling range so that it appears to be a less dominant feature of the positive index PNA pattern.

(*b*) *The western North Pacific*

(i) *Averaged estimates.* The western domain $C_m(l)$ graphs reveal the following structures: With increasing embedding dimension (or delay time m) their slope and thus the dimensionality of the system tends to increase for decreasing distance threshold. For the l range 500 km $< l <$ 1200 km the lower bounds of dimension and entropy can be deduced which, however, should be regarded only as first estimates: $D_2 > 5$ and $1/K_2 < 2$ days, which corresponds to a doubling time between 1 and 2 days. There is no indication that two subsystems govern the storm track dynamics. However, we still need to investigate whether these effects can be related to a particularly persistent flow anomaly of the western North Pacific, which may have been averaged out.

(ii) *Anomalous flow pattern.* The Western Pacific (WP) pattern has a positive sign when the jet over Japan is weaker, that is, when the Aleutian low is weaker or shifted to the east. We might expect cyclones to move more slowly when the WP pattern index is positive. When the WP pattern index is negative we expect the jet to be narrower as well as more intense, so the cyclone tracks may be aligned in a narrower band. Both L and GL find the tracks to be further south at the dateline when WP is positive. For negative WP, L finds much stronger growth than for positive WP. The weaker upper-level trough off the Asian coast (for WP > 0·4) arises because the Aleutian low is weaker or further east. Again, as for the PNA pattern, two groups were selected; one of nine months with a WP index >0·4 and the other of eight months when the WP index is <−0·4 (Table 2). The cyclone track analysis is made for the western North Pacific basin using these two groups.

The phase space scaling of the western Pacific storm tracks does not reveal a notable difference between the high and low index patterns (268 and 244 cyclones, respectively). The $C_m(l)$ graphs are therefore not shown. There is only a slight indication that the storm tracks during low index circulation patterns may also be governed by two subsystems with the scale ranges of 1800 km $< l <$ 3000 km and $l <$ 1800 km (ln(dist) = 7·5 in Fig. 3): in the larger-scale subsystem the weak bounds of dimension and entropy may be estimated $D_2 = 1{\cdot}4$ to $1{\cdot}6$ and $1/K_2 > 7$ to 8 days; for the smaller scales $D_2 > 4$ and $1/K_2$ about 2 days. But these conclusions cannot be regarded as final and the $C_m(l)$ graphs are not shown.

(c) *The Australian region*

The same method of analysis is applied to the mid-latitude storm tracks in the Australian region. The correlation integral estimates shown in Fig. 3 resemble those of the western Pacific average circulation patterns. With increasing embedding dimension (or delay time m) the slope, D_2, of the correlation integral and thus the dimensionality (and unpredictability) of the cyclone track system tends to increase with the embedding and scale. The dimensionality and entropy should be interpreted as first estimates of lower bounds, $D_2 > 5$ and $1/K_2 < 2$ days near 600 km (increasing with distance scale). There is no significant large-scale persistent anomaly pattern in the Australian region which is as predominant as the PNA pattern in the North Pacific basin and could be used to investigate an anomaly dependence of the results.

(d) *Discussion*

A possible reason why the scale separation is observed only in the eastern North Pacific may be the large amplitude disturbances in that area. That is, the scale separation between noise due to limited resolution (inertial gravity modes or geostrophic turbulence) and the low-dimensional Rossby dynamics may be observable only because large amplitude storms define a sufficiently large signal which is controlled by a dynamics with few degrees of freedom. But the western North Pacific, Australian region cyclones appear to be too small and/or governed by too many modes that a distinction between the dynamically relevant modes and noise (or turbulence) from unresolved scales cannot be made in the critical range of about $l = 700$ to 800 km if storm track data are used.

The two subsystems discovered by the fractal analysis of (all tracks of) the eastern North Pacific large amplitude cyclones persist in both the positive and negative index PNA pattern. The larger scales (700 km $< l <$ 2900 km) are associated with a relatively low-dimensional attractor, of whose properties the dimension appears to be different for both PNA patterns.

From a synoptic point of view the positive index is associated over the eastern North Pacific with enhanced westerlies aloft in the area of the storm tracks. This means a stronger baroclinicity and a stronger steering current, which would explain a more rapid divergence of cyclones (and reduced predictability) for the positive than for the negative PNA situations. The deduced predictability time scales indicate such a behaviour. The negative PNA situation can be associated with a stagnation of cyclone positions near the positive Aleutian height anomaly. Such a behaviour is well observed during blocking spells when cyclones slow down as they approach the block and dissipate as they reach it. This could explain the undulations in the $C_m(l)$ graphs (for sufficiently large $l >$ 700 km, Fig. 3(f)), when reaching saturation for increasing embedding m.

The estimates of negative and positive PNA index storm track predictability (order-2 entropy) overlap in their variability in the range 700 km $< l <$ 2900 km. That is, for *short range* forecasts one cannot expect a simple relationship between PNA modes and predictability. Indeed, numerical weather prediction studies over the PNA domain show that the forecast skill does not correlate with any quasi-stationary PNA-like mode (e.g. Palmer 1988; Palmer and Tibaldi 1986), which is at least qualitatively in agreement with our results.

However, medium and extended range predictability (and stability) variations have been observed to depend on the PNA mode (Palmer 1988). This may be related to the changing dimensionality (and not the order-2 entropy, which is a measure of initial error growth) of the attractor on which the dynamical system evolves. A negative PNA index (associated with a lower dimensional attractor) may reduce the medium and extended range predictability (and *vice versa*) under the following scenario: Assume that the dynamics of both negative and positive index PNA patterns evolves on the same energy level which is mixing over two active modes (PNA < 0) or three (PNA > 0); then larger amplitudes of the individual modes are found in the lower-dimensional system and not in the higher-dimensional one. That is, the 2-dimensional energy circle has a larger radius than the (3-dimensional) energy ball. Now, after a sufficiently long lead time the forecast has reached the equilibrium energy level (the hypersurface of the energy circle or ball), and distances on these surfaces represent errors. Then, the distance between randomly chosen points on the circle (with the larger radius) represents a longer term forecast error in the lower-order system. These errors are larger than the random distances on the 3-dimensional ball which is associated with the smaller radius. Note that after a period of medium or extended range the forecast error (approaching saturation) is governed by the nonlinear interactions and is independent of the initial exponential error growth. Thus a reduced medium and extended range predictability (that is larger errors) for the negative PNA situation (with fewer active modes compared with the positive pattern) can occur even if growth rates of initially small errors are the same in both cases.

4.2. Time scaling estimates

The time scaling analysis (described in section 3) is introduced to obtain (Langrangian) measures of a dynamical system which does not reveal a scale preference. The structure functions are averages over individual planar tracks of cyclones (lasting more than three days) and provide the following statistical estimates (section 3, Eqs. (3.3)–(3.5)): (a) the fractal dimension of the tracks covering the latitude–longitude plane; (b) the range of scales for which self-affine (or self-similar) solutions appear to be a valid and useful parametrization of regimes without scale preference; and (c) quantitative measures for this self-affinity and for the related Lagrangian power-law frequency spectra. The results are presented as $\ln\langle(x(t + \lambda T) - x(t))^2\rangle$ versus $\ln \lambda$ graphs (Fig. 4) where x is either latitude or longitude in radians. For self-affine signals, the graphs of the structure function scale linearly with the slope, $2H$, or the scaling exponent, H.

(*a*) *North Pacific basin*

For the total basin cyclone tracks (Fig. 4(a)), the zonal and meridional time scaling exponents are estimated to be of similar magnitude for longitude and latitude, $H = 0{\cdot}8$, which corresponds to the fractal dimension $1/H = 1{\cdot}2$–$1{\cdot}3$ and a power-law spectrum which decreases by $a = 2H + 1 = 2{\cdot}6$ with increasing frequency. The zonal (meridional) scaling of the structure function may be extended as far as 0·45 rad (0·35 rad) and to about 5 days. This can, for example, be compared with results from wavenumber–frequency analyses of daily 500 mb geopotential heights along 50°N in winter (Fraedrich and Böttger 1978, see Fig. 4). The average spectrum of (wavenumber-integrated) variance densities of the zonally propagating waves follows a slope of $2 < a < 3$ towards higher frequencies and may be associated with geostrophic turbulence; $1 < a < 2$ is found for the stationary variance contributions.

The structure function analysis of Pacific storm tracks is in some agreement with results obtained from oceanographic analyses in the Kuroshio extension (Osborne *et al.* 1986), which are based on three freely drifting buoys in the 30–50°N belt from about 135°E to 160°W. The fractal dimensions of the buoy trajectories lie in the interval $1{\cdot}14 < 1/H < 1{\cdot}35$. The oceanographic estimates, however, are limited by the smaller space scale of 150 km of geostrophic turbulence in the ocean and the time scale limit of about a week.

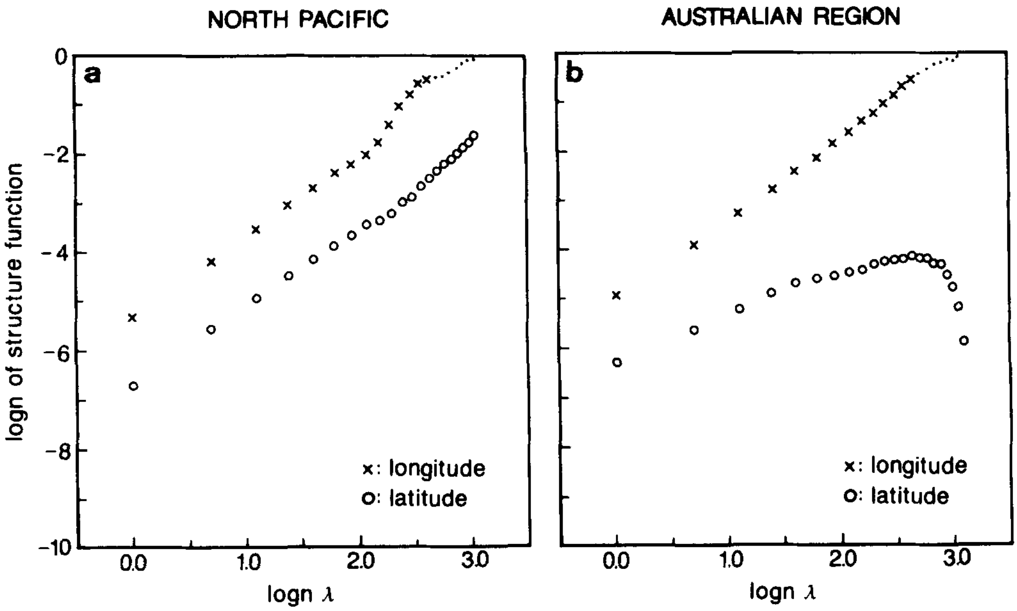

Figure 4. Structure functions of meridional and zonal cyclone displacements displayed in $\ln\langle(x(t+\lambda T)-x(t))^2\rangle$ versus $\ln\lambda$ diagrams (the label logn denotes the natural logarithm) for λ time steps and a sampling time of $T = 12$ hours for the North Pacific cyclone tracks (or one day for the Australian region). The cyclone displacements are given in radians. Cyclone tracks are analysed for the North Pacific basin, (a); and the Australian region, (b).

The analyses of cyclone tracks in the western and eastern North Pacific basins and for the associated anomalies lead to similar results, in particular in the smaller-scale regime, and therefore are not presented.

(*b*) *The Australian region*

The analyses of the North Pacific cyclones (Fig. 4(a)) may be compared with those in the Australian region (Fig. 4(b)). The results for the zonal displacements are very similar. The scaling (for a regime of geostrophic turbulence) extends over a wide range and covers almost the whole life cycle of the storms; the fractal or similarity dimensions are very close, $1/H = 1{\cdot}2$–$1{\cdot}3$, and associated with a similar power law for the frequency spectrum. However, the time scaling regime of the meridional displacements is limited by about 0·1 rad and 2–3 days and leads to a relatively large fractal dimension, $1/H = 1{\cdot}9$. This difference may be related to the dominant zonality of Australian region cyclone tracks (and southern hemisphere dynamics) and the stronger noise modifying the meridional displacements which is due to the topographic influence of the Australian continent.

Finally, a comment on both the fractal and the correlation dimension seems to be in order. The fractal dimension estimates ($1/H$, based on the structure function of planar cyclone tracks) and the associated correlation dimension ($D_2(m = 1)$, obtained from the correlation integrals in the 2-dimensional phase space for zero time lag, that is $m = 1$) are difficult to compare directly: Firstly, the correlation integral depends on distances between independent cyclone tracks whereas the structure function is based on displacements of dependent (individual) tracks only. The correlation integral describes a phase space scaling whereas the structure function characterizes a time scaling. Second, the estimate of $D_2(m = 1) = 1{\cdot}6$ ($1{\cdot}9$) in the North Pacific (Australian) basin is valid for distances smaller than 2000 km. The related fractal or similarity dimension obtained from the structure function scaling is of smaller magnitude, $1/H = 1{\cdot}2$ to $1{\cdot}3$, and covers almost the whole life cycle of the storms (except for the Australian cyclones' meridional displacements, which have been explained). It appears that the averaging over independent pairs of tracks tends to weight the randomness in the $m = 1$ correlation dimension estimate $D_2(m = 1)$ which, therefore, turns out to be larger. And last it should be mentioned (Osborne and Provencale 1989) that a finite correlation dimension from observational data does not necessarily imply the presence of deterministic chaos as there are stochastic processes with a finite value of the fractal dimension.

5. Conclusions

Estimates have been made of the predictability characteristics of mid-latitude cyclone tracks in the North Pacific and the Australian Southern Ocean region, using recently developed techniques for the analysis of nonlinear dynamical systems. This work follows on from a previous study (part I, Fraedrich and Leslie 1989) in which phase space scaling methods were employed to provide estimates of the dimensionality and error doubling time scales for tropical cyclone tracks in the Australian tropics.

In this study, scaling of the cyclone tracks in a substitute phase space was used to provide estimates of dimensionality and error doubling time scales for mid-latitude cyclones. For the North Pacific region there were three main results.

Firstly, it was found that in the eastern North Pacific there is a 'knee' in the correlation integrals which divides the systems into two distinct scales or regimes. These scales are greater than about 700 km and less than 700 km. The larger-scale subsystem was found to have an error doubling time of roughly three or four days whereas the smaller-scale subsystem appears to be characterized by noise or geostrophic turbulence as the dimensionality does not reach a saturation value.

Secondly, it was found that for the eastern North Pacific the structure of the correlation integral depends on the sign of the Pacific/North American anomaly index. For negative values of the PNA index the dimensionality of the larger-scale subsystem is very low and the predictability time scale is about 3–5 days. The smaller-scale subsystem has a dimensionality much greater and a very short predictability time scale of about one to two days. When the PNA index is positive there appears to be no such clear distinction in dimensionality and predictability between the large- and the small-scale subsystems.

Thirdly, in the western North Pacific and the Australian Southern Ocean, the correlation integrals reveal no 'knee' and no apparent dependence, in the case of the western North Pacific cyclones, on circulation anomalies.

Furthermore, a time scaling analysis of cyclone tracks is applied to deduce time structures of dynamical regimes which are characterized by a lack of scale preference. The Lagrangian structure functions of individual tracks reveal a scaling behaviour which corresponds with the frequency spectra of zonally propagating waves in the geopotential height fields. Both analyses follow a power-law spectrum which decreases by a 2–3 slope with increasing frequency. Data of drifting buoys in the North Pacific Ocean show a comparable scaling behaviour.

Finally, some comments on the limitations of these analyses are in order: (i) The life-cycle or tracks of the cyclones may not last sufficiently long to completely cover the attractor embedded in the substitute phase space spanned by the delay coordinates; note, however, that the analysis is spanned by delayed vector coordinates and not the commonly used lagged single variable time series. (ii) Some care is needed in the literal interpretation of the estimates because the evaluation of the correlation integrals and structure functions is partially subjective. (iii) Physical explanations, in particular for the PNA-dependence of the attractor dimension (and entropy), are beyond the scope of this analysis, because it is possible to determine the number, but not which of the atmospheric modes are actively involved in the deterministic dynamics governing the PNA-related storm track behaviour.

Acknowledgements

The North Pacific data were graciously provided by the Data Support Section of the National Center for Atmospheric Research (NCAR). The North Pacific storm tracks were calculated by Mr S.-S. Lai using the computing facility at NCAR. Post processing was performed at BMRC by Mr M. Whimpey; Mr Whimpey also performed the computations using the Australian region data archives at BMRC. Mr H. Nakamura kindly provided the anomaly indices shown in Table 1. Mr H. Haug did part of the drafting. One of the authors (RG) was supported by the U.S. National Science Foundation grant ATM 86-06267. Finally, the comments of two referees helped to clarify the results and were appreciated.

Appendix

Interpolation scheme for North Pacific storm tracks

The original data were archived on a polar stereographic grid covering most of the northern hemisphere. The 63 by 63 grid has about 381 km resolution at 60°N. These data were interpolated onto an equally-spaced latitude–longitude grid extending from 95°E to 255°E and 20°N and 80°N. The equally-spaced grid will be called the L grid; it used a 2·5° grid interval, which was higher resolution than the stereographic grid in the northern part of the domain. Since we were mainly interested in finding the storm centres and not the central pressures, the higher resolution was allowable, and useful. The storm tracks were found by a combination of iterative time and space interpolation procedures as follows:

First, the data were linearly interpolated to a time interval of 2 hours to improve the accuracy of matching the centre of the same storm at successive times. Over two hours, storms move small distances compared with the distances separating the storms. Using a 12-hour interval it is much harder to automate a procedure that avoids confusing one storm with another. The problem with linear time interpolation is that fast-moving, weak systems could be missed at times mid-way between the original 12-hour observations (see discussion in Grotjahn and Wang 1988). Occasionally, storms were missed in just this way, and a gap would appear between two tracks that were clearly from the same storm. However, the storm tracks were post-processed (by extrapolating the two pieces forwards and backwards in time) to identify and link up such tracks.

Next, relative maxima at grid points on our equally spaced L grid were identified. If the sea-level pressure (s.l.p.) of a minimum was less than 1010 mb, then a further search was carried out around the given grid point.

Finally, the search consisted of five iterations. Each required interpolation of s.l.p. values onto a square grid of 9 points centred upon the minimum s.l.p. found during the previous iteration. The interval between the points on the small square grid was halved with each iteration. The location of the minimum s.l.p. on the final iteration was stored.

The storm tracks at 2-hour intervals for each January and February from 1972 through 1982, and 1984 through 1986 were calculated in this manner. In addition, only the first 19 days of January 1983 were available.

References

Allen, R. A., Fletcher, R., Holmboe, J., Namias, J. and Willett, H. C. 1940 Report on an experiment on five-day weather forecasting. *Pap. Phys. Oceanogr. Meteorol.*, MIT/WHOI, 8

Dickson, R. R. and Namias, J. 1976 North American influences on the circulation and climate of the North Atlantic sector. *Mon. Weather Rev.*, **104,** 1255–1265

Eckmann, J. P. and Ruelle, D. 1985 Ergodic theory of chaos and strange attractors. *Rev. Mod. Phys.*, **57,** 617–656

Fraedrich, K. 1987 Estimating weather and climate predictability on attractors. *J. Atmos. Sci.*, **44,** 722–728

Fraedrich, K. and Böttger, H. 1978 A wavenumber-frequency analysis of the 500 mb geopotential at 50°N. *ibid.*, **35,** 745–750

Fraedrich, K. and Leslie, L. M. 1989 Estimates of cyclone track predictability. I: Tropical cyclones in the Australian region. *Q. J. R. Meteorol. Soc.*, **115,** 79–92

Grassberger, P. and Procaccia, I. 1984 Dimensions and entropies of strange attractors from a fluctuating dynamics approach. *Physica*, **13D,** 34–54

Grotjahn, R. and Lai, S.-S. 1989 'Storm tracks over the North Pacific grouped by climate anomalies during 22 winters.' University of California at Davis. Atmos. Sci. Group Tech. Note 100015.

Grotjahn, R. and Wang, C.-H. 1988 On the source of air modified by ocean surface fluxes to enhance frontal cyclone development. *Ocean–Air Interactions*, **1,** 257–288

Kalnay, E. and Dalcher, A. 1987 Forecasting forecast skill. *Mon. Weather Rev.*, **115,** 349–356

Kalnay, E. and Livezey, R. 1985 Weather predictability beyond a week. Pp. 311–346 in *Turbulence and predictability in geophysical fluid dynamics and climate dynamics*. M. Ghil, R. Benzi and G. Parisi, Eds. North Holland

Lau, N.-C. 1978 On the three-dimensional structure of the observed transient eddy statistic of the Northern Hemisphere wintertime circulation. *J. Atmos. Sci.*, **35,** 1900–1923

1988 Variability of the observed mid-latitude storm tracks in relation to low-frequency changes in the circulation pattern. *ibid.*, **45,** 2718–2743

Lorenz, E. N. 1969 The predictability of a flow which possesses many scales of motion. *Tellus*, **21,** 289–307

1986 On the existence of a slow manifold. *J. Atmos. Sci.*, **43,** 1547–1557

Lorenz, E. N. and Krishnamurthy, V. 1987 On the nonexistence of a slow manifold. *ibid.*, **44,** 2940–2950

Lovejoy, S. and Schertzer, D. 1986 Scale invariance, symmetries, fractals, and stochastic simulations of atmospheric phenomena. *Bull. Am. Meteorol. Soc.*, **67,** 21–32

Mandelbrot, B. 1982 *The fractal geometry of nature.* Freeman and Co., New York

Monin, A. S. and Yaglom, A. M. 1975 *Statistical fluid mechanics.* Vol. 2. The MIT Press

Nakamura, H., Tanaka, M. and Wallace, J. M. 1987 Horizontal structure and energetics of Northern Hemisphere wintertime teleconnection patterns. *J. Atmos. Sci.*, **44,** 3377–3391

Namias, J. 1951 The great Pacific anticyclone of the winter 1948–50: A case study in the evolution of climatic anomalies *J. Meteorol.*, **8,** 251–261

Osborne, A. R. and Provencale, A. 1989 Finite correlation dimension for stochastic systems with power-law spectra. *Physica*, **35D,** 357–381

Osborne, A. R., Kirwan, A. D., Provencale, A. and Bergamasco, L. 1986 A search for chaotic behaviour in large and mesoscale motions in the Pacific Ocean. *ibid.*, **23D,** 75–83

Palmer, T. N. 1988 Medium and extended range predictability and stability of the Pacific/North American mode. *Q. J. R. Meteorol. Soc.*, **114,** 691–713

Palmer, T. N. and Tibaldi, S. 1986 'Forecast skill and predictability'. ECMWF Technical Memorandum No. 127

Shukla, J. 1984 Predictability of a large atmospheric model. Pp. 449–456 in *Predictability of fluid motions.* Holloway, G. and West, B. J., Eds. American Institute of Physics, New York

Smagorinsky, J. 1969 Problems and promises of deterministic extended range forecasting. *Bull. Am. Meteorol. Soc.*, **50,** 286–311

Thompson, P. D. 1957 Uncertainty of the initial state as a factor in the predictability of atmospheric flow patterns. *Tellus*, **9,** 275–295

Voss, R. V. 1988 Fractals in nature. Pp. 21–70 in *The science of fractal images*. Peitgen, H.-O. and Saupe, D. Eds. Springer-Verlag

Wallace, J. M. and Gutzler, D. S. 1981 Teleconnections in the geopotential height field during the Northern Hemisphere winter. *Mon. Weather Rev.*, **109,** 784–812